UNIVERSIDADE FEDERAL DA PARAÍBA

CENTRO DE CIÊNCIAS DA SAÚDE

PROGRAMA DE PÓS-GRADUAÇÃO EM ODONTOLOGIA

ESTUDO QUANTITATIVO DA PERMEABILIDADE DE LESÕES CARIOSAS NATURAIS DE ESMALTE À SOLUÇÃO DE THOULET

Kássia Regina Simões Meira

2014

KÁSSIA REGINA SIMÕES MEIRA

ESTUDO QUANTITATIVO DA PERMEABILIDADE DE LESÕES CARIOSAS NATURAIS DE ESMALTE À SOLUÇÃO DE THOULET

Dissertação apresentada ao Programa de Pós-Graduação em Odontologia, da Universidade Federal da Paraíba, como parte dos requisitos para obtenção do título de Mestre em Odontologia – Área de Concentração em Odontologia Preventiva e Infantil.

Orientador: Prof. Dr. Frederico Barbosa de Sousa.

Co-Orientador: Prof. Dr. Hugo Lemes Carlo

João Pessoa

2014

M514e Meira, Kássia Regina Simões.
Estudo quantitativo da permeabilidade de lesões cariosas naturais de esmalte à solução de Thoulet / Kássia Regina Simões Meira.-- João Pessoa, 2014.
53f. : il.
Orientador: Frederico Barbosa de Sousa
Coorientador: Hugo Lemes Carlo
Dissertação (Mestrado) - UFPB/CCS
1. Odontologia. 2. Odontologia preventiva e infantil. 3.Cárie dental. 4. Esmalte. 5. Histologia. 6. Permeabilidade.

UFPB/BC CDU: 616.314(043)

KÁSSIA REGINA SIMÕES MEIRA

ESTUDO QUANTITATIVO DA PERMEABILIDADE DE LESÕES CARIOSAS NATURAIS DE ESMALTE À SOLUÇÃO DE THOULET

Banca Examinadora

Prof. Dr. Frederico Barbosa de Sousa

Orientador - UFPB

Prof. Dra. Ana Maria Barros Chaves

Examinador - UFPB

Prof. Dra. Aline de Almeida Neves

Examinador - UNIGRANRIO

DEDICATÓRIA

À Regina Simões, minha avó materna, a jóia mais preciosa da minha vida. Dedico todo meu esforço para a realização dessa conquista em agradecimento à educação, ao amor infinito e acima de tudo ao exemplo de vida que é para mim.

AGRADECIMENTOS

À **Deus**, por me fazer suportar nesse grande desafio. Quando mais precisei estar próximo da minha família e do meu lar, no momento mais doloroso, o Senhor me afasta de tudo e me dar asas para que eu pudesse voar sozinha e seguir em frente. Obrigada Papai do Céu por essa nova chance de viver.

Aos meus pais, **Dorinha e Zé Mário**, que sofreram comigo a dor da distância, mas que sempre acreditaram que eu venceria os maiores obstáculos. Mainha e Painho, à vocês devo minha vida. Obrigada pela confiança, pela fé, por minha educação e pelo amor infinito. Amo vocês.

À minha família **Simões Meira**, em especial às minhas irmãs **Karla** e **Keyla** por estarem presentes nos momentos bons e ruis. Essa vitória também é de vocês.

Ao meu orientador, **Prof. Dr. Frederico,** pela confiança depositada em minhas mãos e por tantos ensinamentos. A jornada foi longa, mas o resultado foi mais que satisfatório. Muito obrigada pela oportunidade.

Ao meu namorado, **Rafael Almeida**, pela paciência, pelo incentivo, companheirismo, confiança e acima de tudo, pelo amor que nos une.

À família **Bozi Ramalho**, minha família de coração que me acolheu como uma filha. Serei grata por toda minha vida por tudo que vocês fizeram por mim. Muito obrigada: **Regina, Genival, Daniel, Daniely, Bruno, Joel e Camila**.

À **Camila Brito** e **Danilo Augusto**, verdadeiros irmãos que Deus colocou em minha vida. Que nossa amizade se fortaleça com o passar dos dias.

Aos **amigos do mestrado**, em especial àquelas que têm um cantinho especial no meu coração: **Aretha, Palmira, Julyana, Jossaria, Patrícia e Laudenice**, que além de excelentes profissionais são companheiras para todas as horas.

Aos colegas do **LAMIB**, que acompanharam de perto toda a pesquisa, dando apoio e ajudando no que fosse necessário. Obrigada **Fernanda, Manu, Lúcia, Plínio e Adami**.

À colega **Laudenice,** sem sua ajuda essa pesquisa não seria realizada, obrigada por contribuir com a amostra do estudo.

Aos professores e ex-professores das Faculdades Integradas de Patos (FIP), por acreditarem que eu tinha potencial para chegar até aqui. Muito obrigada pelo apoio: **Andreza Targino, Jocianelle Nunes, Sérgio Henrique, Fátima Roneiva e Fernando Aires.**

Aos **meus amigos**, os melhores que alguém pode ter, mesmo perto ou longe sinto o imenso carinho e apoio de cada um de vocês, muito obrigada por estarem presentes em um momento tão importante na minha vida.

"Mesmo quando tudo parece desabar, cabe a mim decidir entre rir ou chorar, ir ou ficar, desistir ou lutar; porque descobri, no caminho incerto da vida, que o mais importante é o decidir."

RESUMO

Em lesões cariosas naturais de esmalte, os agentes terapêuticos que promovem a remineralização e infiltração do esmalte desmineralizado por resina dependem diretamente da permeabilidade do tecido. A camada superficial tem sido considerada uma barreira para penetração desses agentes devido à sua baixa permeabilidade. Neste estudo, pela primeira vez, são fornecidos dados volumétricos quantitativos sobre a infiltração de uma solução teste (solução aquosa de iodeto de mercúrio e de potássio - Solução de Thoulet) na camada superficial da lesão cariosa natural de esmalte. Confirmou-se a hipótese de que a razão do volume de água ao quadrado dividido pelo volume de poros (α_d) é dentre todos os volumes (mineral, orgânico, água total e água fracamente aderida), o melhor preditor da proporção do volume de poros infiltrados pelas soluções testadas. O valor preditivo de α_d foi maior pra Solução de Thoulet com índice de refração 1,47 (R2= 0,505) em comparação à Solução de Thoulet com índice de refração 1,40 (R2= 0,435). O mapeamento em 2D da infiltração em tempo real revelou que a penetração da solução começou inicialmente através da superfície do esmalte, seguindo para o interior do corpo da lesão seguindo a trajetória dos prismas e provocando um fluxo de ar no sentido oposto. A infiltração foi insignificante através dos poros nas superfícies expostas por desgaste. Dados sobre os volumes efetivos, viscosidade e da mecânica do fluxo de fluidos nos poros, forneceram informações nunca antes publicadas sobre a natureza da infiltração de materiais na camada superficial e lesão cariosa natural de esmalte. O presente estudo pode fornecer uma visão mais profunda sobre o transporte de agentes usados para a remineralização e infiltração de resinas na lesão cariosa natural de esmalte.

Palavras-chave: Esmalte; Cárie dental; Histologia; Permeabilidade

ABSTRACT

In natural enamel caries, remineralization and resin infiltration are directly dependent on the permeability of the enamel to the agents that promote them. Due to its low permeability, the surface layer of carious lesions has been considered, a natural barrier for penetration of such agents. In this study we provide, for the first time, quantitative volumetric data on the infiltration of a test solution (aqueous solution of mercuric and potassium iodide: Thoulet's solutions) in the surface layer of natural enamel caries and confirmed our hypothesis that the ratio of the squared water volume by pore volume (α_d) is, among all major component volumes (mineral, organic, total water and loosely bound water), the best predictor of the proportion of the pore volume infiltrated by the tested solutions. The predictive value of α_d was higher for Thoulet's solution with refractive index 1.47 (R^2 = 0.505) compared to Thoulet's solution with refractive index 1.40 (R^2=0.435). Real-time 2D mapping of infiltration revealed that penetration of the solution started on the original enamel surface, followed the prism paths towards the bottom of the body of the lesion, and caused air flow in the opposite direction. Infiltration was negligible through the pores at the surfaces exposed by cutting and grinding. Data on effective pore volume, pore viscosity and from fluid flow mechanics provided new information on the nature of the infiltration of materials in the surface layer of natural enamel caries. Our results might provide a deeper insight into the transport of agents used to promote remineralization and resin infiltration in natural enamel caries.

Keywords: Enamel; Dental Caries; Histology; Permeability

SUMÁRIO

1. INTRODUÇÃO

O esmalte, que recobre a coroa do elemento dental e que sofre os primeiros efeitos do biofilme cariogênico em indivíduos jovens, é o tecido mais mineralizado do corpo humano, apresentando volume mineral próximo a 90%. O remanescente é constituído por matéria orgânica e água.[12,34,16]

O componente mineral do esmalte encontra-se na forma de cristais alongados de hidroxiapatita que, em sua maioria, percorrem toda a espessura do esmalte (desde a junção com a dentina até a sua do esmalte). Esses cristais têm largura de 60-70 nm e espessura de 25-30 nm, e são compactados em colunas definidas como prismas[36,18]. A espessura do esmalte varia com a localização, apresentando espessura máxima de 2,5 mm nas regiões de borda incisal e pontas de cúspides. Aproximando-se da região cervical o esmalte vai tornando-se mais delgado.[4]

O arranjo dos cristais no esmalte dá origem a duas categorias principais de poros: uma formada por poros que se encontram no interior dos prismas e do esmalte interprismático (entre os cristais de hidroxiapatita) e possuem diâmetros de 1-2 nm; e outra formada por poros que se encontram logo nos arredores de cada prisma (bainhas entre os esmaltes prismático e interprismático), com 4-6 nm de diâmetro. Todos os espaços intercristalinos são preenchidos por água mais componentes orgânicos hidrofóbicos e hidrofílicos representados por lipídios e proteínas[23,36], e estes componentes orgânicos provavelmente estão em contato direto com a hidroxiapatita[28,15]. A água encontrada no interior dos poros é chamada de água livre e se encontra sob duas formas: fracamente aderida, relacionada ao volume orgânico, e fortemente aderida, relacionada ao volume mineral[5,12]. A diferença entre as duas é que a primeira é removida com menos energia (à temperatura ambiente, por exemplo). O conjunto dos espaços intercristalinos forma um sistema complexo, tortuoso e seletivamente permeável de nanocanais interligados por onde se dá o transporte de materiais no esmalte.

O poro é reduzido pela presença de proteínas, sendo que a hidratação desta pode reduzir a mobilidade da água dentro dos poros e alterar a difusão de solutos através de interações com a carga das proteínas. Além disso, o

componente lipídico pode influenciar a difusão de solutos de acordo com sua hidrofobicidade[29].

Sendo assim, o esmalte pode ser classificado como uma membrana semipermeável formada de poros que formam um sistema microscópico de "túbulos/cilindros" interligados em que a água é transportada para o interior do tecido sob um gradiente osmótico, podendo também haver transporte de solutos na direção oposta[29]. Esse sistema de transporte através do esmalte é importante para várias de suas propriedades físico-químicas como elasticidade, permeabilidade, reatividade, trocas iônicas e também têm papel no processo de transporte de drogas (como por exemplo, agentes clareadores), de produtos bacterianos e de materiais restauradores. *In* vivo, esse transporte ocorre através de difusão

A difusão é o principal mecanismo de transporte no esmalte[29]. Fluxo não ocorre devido ao fato de que este é inversamente proporcional à quarta potência do diâmetro dos poros, o que resulta que pressões altíssimas seriam necessárias para induzir fluxo nos poros com diâmetros nanométricos encontrados no esmalte. A água do esmalte se difunde em direção à junção amelo-dentinária, sob influência de um gradiente osmótico[1]. Evidências recentes indicam que existe uma maior concentração de matéria orgânica nos poros mais internos do esmalte (100-400 μm)[14], que devem exercer um papel na criação desse gradiente osmótico, cujo resultado é a difusão da água em direção à camada mais interna do esmalte.

Assim, é importante destacar a equação de difusão proposta por Einstein[13]:

$$D = \frac{R \cdot T}{N_A 6\pi\eta a} \quad (1)$$

Onde R é a constante universal dos gases, T é a temperatura absoluta (Kelvin), N_A é o número de Avogrado, η é a viscosidade ($m^{-1}Kgs^{-1}$) e a é o tamanho da molécula.

Esta equação prever que a taxa de difusão é inversamente proporcional ao diâmetro dos poros e à viscosidade do meio. Assim, a difusão nos poros intra-prismáticos deve ser menor do que aquela nas bainhas. E a difusão para o interior da matéria orgânica no esmalte desidratado deve ser menor porque a contração daquela cria um meio mais viscoso (mesma quantidade de matéria orgânica para um menor volume de água). Isto ressalta a importância de se saber o volume dos poros preenchido pelo material infiltrante. Uma vez que a matéria orgânica não sai, quanto maior a penetração menor a permeabilidade do volume que não foi infiltrado. Isto é muito importante para infiltração resinosa e remineralização de lesões cariosas.

Assim, o transporte de ácido proveniente do biofilme dental se dá por difusão através do ambiente heterogêneo dos poros do esmalte. Durante o deslocamento, o ácido penetra no tecido e interage com seus componentes químicos. A formação da lesão cariosa resulta de dois processos parcialmente independentes: penetração do ácido e desmineralização[30]. A penetração, definida como o processo de dissolução do material nas bainhas dos prismas pela difusão rápida do ácido, ocorre com pouca perda mineral, mas com um aumento significativo dos poros das bainhas. A desmineralização, perda mineral principalmente no interior dos prismas, é resultado de uma difusão lenta do ácido nos poros intra-prismáticos. Ressalta o autor que a penetração não ocorre totalmente sem desmineralização. Assim, a dissolução cariosa do esmalte é grandemente influenciada pela distribuição anatômica e largura das bainhas.[30]

Pelo papel crucial da difusão na patogênese da lesão cariosa do esmalte, fica claro que as características histopatológicas da lesão cariosa de esmalte foram descritas com base nas variações da permeabilidade do esmalte cariado. Devido a birrefringência do esmalte ser muito sensível a variações nos volumes e nos índices de refração do mineral e de poros[9,34], e estes poros serem permeáveis a líquidos com diferentes índices de refração, a microscopia de luz polarizada se tornou uma ferramenta muito importante no estudo da distribuição de poros na lesão cariosa de esmalte.

Uma vez que a birrefringência requer uma interpretação matemática, um modelo simplificado, mas que se mostrou bastante razoável na época foi

proposto por Darling (1956). Neste modelo, os poros do esmalte não contêm matéria orgânica e se considera que toda a água livre é facilmente removida pela desidratação à temperatura ambiente (cerca de 20º C). Apesar de não ser consistente com a real composição do esmalte, este modelo permitiu separar zonas na lesão cariosa do esmalte relacionadas a diferentes porosidades estimadas a partir da infiltração de determinadas soluções após certo tempo. Estas porosidades implicam em diferentes permeabilidades, isto porque este procedimento envolveu o transporte de certa massa nos poros do esmalte em função do tempo e a unidade de permeabilidade é mol x m^{-1} x s^{-1} x Pa^{-1} [26].

A primeira evidência macroscópica de cárie pode ser vista em um dente como uma pequena área branco-opaca[32]. Nas lesões que se encontram neste estágio, foram descritos, com base nas imagens de microscopia de luz polarizada, quatro zonas histopatológicas de porosidade relacionadas com a lesão de cárie[9,11]:

- Zona translúcida: é a camada mais profunda da lesão, onde ocorre a primeira mudança visível no esmalte cariado, apresentando uma perda de ~ 1% de volume mineral e poros relativamente grandes;

- Zona escura: fica adjacente à zona translúcida, apresentando uma mistura de poros grandes e pequenos, sendo o volume de poros de 2-4%;

- Corpo da lesão: é a zona com maior perda mineral, apresentando volume de poros de 25-50%, sendo eles em sua grande maioria constituído de poros de grandes dimensões.

- Camada superficial: é a camada mais externa da lesão, apresentando volume de poros de menos de 5 %. Por apresentar birrefringência negativa quando sob imersão em água, idêntica ao esmalte normal, foi descrita como sendo uma zona relativamente “intacta”. Esta camada persiste até a cavitação.[11,33,19]

Os diferentes volumes/tamanhos de poros implicam em diferentes permeabilidades. A camada superficial é a porta de entrada para materiais externos ao esmalte. Por isso, sua permeabilidade é de grande importância quando se trata do transporte de agentes remineralizadores (para reparar o

conteúdo mineral perdido) e/ou resinas infiltrantes (para paralisar as lesões). Consistente com esta afirmação, a remoção da camada superficial foi mostrada como importante para a penetração de resinas infiltrantes em lesões cariosas de esmalte[22] e foi sugerida para aprimorar a remineralização dessas lesões.[8]

Atualmente, a radiomicrografia é a técnica padrão-ouro para se obter inferências sobre as variações na quantidade de poros (e consequentemente na permeabilidade) em pontos histológicos de uma lesão cariosa de esmalte[7]. Uma vez o volume de poros da camada superficial do esmalte cariado determinado pela interpretação da birrefringência pelo modelo de Darling (1956) não têm concordância com o volume mineral quantificado pela radiomicrografia[3], esforços recentes têm sido feitos no sentido de se estipular critérios objetivos de determinação da espessura da camada superficial pelo volume mineral. Cochrane; Andreson; Davis; Adams; Stacey; Reynolds (2012) propuseram que a espessura da camada superficial fosse definida como a distância entre o início da lesão até o ponto com maior conteúdo mineral encontrado antes do centro do corpo da lesão. Esta definição tem implicações na discussão sobre a melhor maneira de remover esta camada com finalidade de potencializar remineralização/infiltração.

Há evidências indicando que variações no conteúdo mineral podem não explicar completamente a permeabilidade da camada superficial nas lesões cariosas de esmalte. Foi relatado que a permeabilidade de lesões cariosas naturais é menor do que em lesões cariosas artificiais com conteúdos minerais supostamente semelhantes, sugerindo um papel da matéria orgânica na permeabilidade do esmalte cariado[22]. Consistente com isto, recentemente foi relatado um maior volume de matéria orgânica na camada superficial em relação ao corpo da lesão[21], o que não pode ser ignorado ao se tentar explicar as diferenças de permeabilidade entre a camada superficial e o corpo da lesão. É possível, por exemplo, que existam poros menores na camada superficial mesmo que esta não apresente volumes minerais maiores que aqueles do corpo da lesão.

As quantidades de água e matéria orgânica são decisivas para determinar a permeabilidade de poros com mesmo diâmetro. A remoção de

matéria orgânica tende a aumentar a permeabilidade. A vantagem desta medida é que ela não requer perda mineral, preservando mais a estrutura do esmalte. Remover matéria orgânica tende a aumentar a quantidade de água fracamente aderida. Uma das grandes dificuldades do esmalte cariado é que sua desidratação deixa-o opaco (sem birrefringência), impossibilitando a quantificação da água fracamente aderida. Para contornar este problema no sentido de permitir quantificar a permeabilidade no esmalte cariado, Barbosa de Sousa; Dias Soares; Sampaio Vianna (2013) propuseram um parâmetro (volume de água total ao quadrado dividido pelo volume não mineral) que supostamente seria relacionado à permeabilidade. Os dados para o calculo deste parâmetro podem ser mensurado em esmalte cariado imerso em água, que dificilmente fica opaco.

O objetivo deste estudo foi testar a hipótese de que a água fracamente aderida é entre todos os volumes dos componentes do esmalte, o melhor preditor do volume de poros infiltrados por um material teste na camada superficial da lesão cariosa natural de esmalte. O material testado aqui foi uma solução aquosa com elevado índice de refração (solução de Thoulet).

2. CAPÍTULO 1

O manuscrito a seguir foi submetido para publicação no periódico "**Acta Biomaterialia"** e encontra-se em revisão por pares

Natural enamel caries: predicting permeability of the surface layer

Kássia Regina [1]

Camila Brito [1]

Frederico Barbosa de Sousa[1,2,3*]

[1] Master program in Dentistry, Health Sciences Center, Federal University of Paraiba, Cidade Universitária, 58051-900, João Pessoa, Paraiba, Brazil.

[2] Laboratory of Microscopy and Biological Image, Health Sciences Center, Federal University of Paraiba, Cidade Universitária, 58051-900, João Pessoa, Paraiba, Brazil.

[3] Department of Morphology, Health Science Center, Federal University of Paraiba, Cidade Universitária, 58051-900, João Pessoa, Paraiba, Brazil

***Corresponding author:**

Frederico Barbosa de Sousa

Departamento de Morfologia, Centro de Ciências da Saúde, Universidade Federal da Paraíba, Cidade Universitária, S/N, CEP 58051-900, João Pessoa, Paraíba, Brazil

Tel: +55-83-3216-7254; Fax: +55-83-3216-7094; E-mail: fredericosousa@hotmail.com

Abstract

In natural enamel caries (NEC) remineralization and resin infiltration are directly dependent on the permeability of the surface layer to the terapeutic agents that promote them. The surface layer (SL) has been considered, because of its low permeability, a strong barrier for penetration of such agents. In this study we provide, quantitative volumetric data on the infiltration of a test solution (aqueous solution of mercuric and potassium iodide - Thoulet's solution) in the SL of NEC. The test hypothesis that the ratio of the squared water volume by pore volume is, among all major component volumes (mineral, organic, total water and loosely bound water), the best predictor of the proportion of the pore volume infiltrated by the tested solutions was confirmed. Real-time 2D mapping of infiltration revealed that penetration of the solution started through the original enamel surface, followed prism paths towards the bottom of the body of the lesion, and caused air flow in the opposite direction. Infiltration was negligible through the pores at the surfaces exposed by cutting and grinding. Data on effective pore volume, pore viscosity and from fluid flow mechanics provided new information on the nature of the infiltration of materials in the SL of NEC.

Keywords: enamel; dental caries; histology; permeability

1. Introduction

The carious process causes in dental enamel a complex network of nano-scaled, albeit larger-than-normal pores. The option of treating incipiente enamel caries (NEC) lesion by arresting further development and reducing pore size has long been searched. Those treatment options do not precinde surgical removal of dental tissue and are thus referred as non-invasive treatment. Reduction of pore size can be achieved by remineralization [1] or infiltration of the pores with fluid resins (known as infiltrants) [2]. The outcomes of such treatments depend, among other factors, on the easy in which remineralizing agents and infiltrants penetrate into NEC. Evidence indicates deeper parts of that the surface layer of NEC might reduce the penetration of materials into NEC. Its removal has been shown to be important for proper penetration of infiltrants into NEC [3, 4], and increased penetration remineralizing materials has been achieved by procedures involving demineralization [for review see 1] and removal of organic matter [5]. In active NEC, which have a more porous surface layer [6], it is known that infiltrants penetrate deeper into NEC when they are active or when inactive lesions are pretreated with acid (to enhance pore sizes) [7]. As it has been recently highlighted, development of procedures to increase penetration of materials through the surface layer of NEC will represent a significant advance in clinical remineralization [1] (and infiltration as well). For the sake of preserving more tissue over time, it has been recently highlighted that preserving the surface layer of NEC should be preferred than acid pretreatment [7].

In this context, it is of paramount important to measure the permeability of the surface layer and to predict the proportion of the pores that will be penetrated by a given material in a surface layer with a given permeability. Because transport in enamel is mainly by diffusion [8, 9], and the diffusion rate is inversely related to the viscosities of both the pore and the infiltrating material [10], it is important to quantify the pore volume which is not penetrated by a given material and how much water and organic matter are present. In this way, pretreatments of the surface layer aimed at enhancing penetration of materials into NEC could be deeper investigated. One of the main challenges to achieve this is to obtain

quantitative volumetric data on the components (mineral, water, and organic matter) of the pores at points with specific histological location in NEC. Recently, our group reported such data [11, 12]. The next big challenge was to measure permeability with spatial resolution in NEC. It is known that water, the main component for diffusion in enamel, is found in the pores divided into two parts, firmly and loosely bound water, and the later has been shown to be related to a faster diffusion rate [13, 14] and, thus can be regarded as the best candidate for a parameter of permeability in enamel. The methodology recently reported [11, 12] is not able to measure loosely bound water in NEC because when loosely bound water is removed by air-drying at room temperature (a necessary step) the sizes of the pores filled only with air increase to an extent that results in opacity in a large part of the lesion (including the surface layer is most cases), avoiding any measurement of birefringence (required for measuring enamel component volumes). To circumvent this, it was measured in NEC the water more easily available for diffusion, proposed to be related to permeability [12].

The aim of this study was to test the hypothesis that the loosely bound water is easily available is among all enamel component volumes, the best predictor of the pore volume infiltrated by a test material in the surface layer of NEC. The material tested here was an aqueous solution with high refractive index (Thoulet´s solution), previously used to define histological layers of NEC under polarizing microscopy [15].

2. Materials and methods

2.1 Samples

Twenty-one noncavitated approximal inactive NEC lesions from human third molars and premolars, extracted for clinical reasons, were selected. Lesion activity was determined by a consensus from examiners calibrated (intra-examiners kappa 0.739 and 0.856; inter-examiner kappa 0.812) with regard to the ICDAS system applied to a pool (30 lesions) of noncavitated NEC lesions that were analyzed under the stereomicroscope after removal of organic cover (1% sodium

hypochlorite for 30 seconds) and air drying with compressed air (10 seconds). This study was approved by the Ethical Committee on Research in Humans of the Lauro Wanderley University Hospital (Federal University of Paraiba, Brazil), and all teeth were donated with signed consent by adult volunteers. Teeth and ground sections were kept in 0.02% aqueous sodium azide solution before and after infiltration experiments with the test solutions. Longitudinal sections were obtained of the approximal surfaces with NEC using a diamond disc under water irrigation. Then, each section was ground down to a thickness of 50-90 µm using a lapping jig as described recently [11]. Sample thickness at the histological points selected for analysis were measured with the sections positioned edge-on in a transmitted light polarizing microscope equipped with a reticle and a 20X objective (resolution of 0.7 µm).

2.1 Quantification of mineral volume

Glass plates sensitive to X-rays (resolution of 2000 lines/mm; AGHD, Microchrome Tech., San Jose, USA) were covered by all ground sections and an aluminum step-wedge calibration standard (10 sheets, each with thickness of 20 µm and purity of 0.999%; ESPI Chemicals, USA) and exposed to X-rays in a PCBA Inspector (General Electric, Germany; Tungsten anode filtered by 0.254 mm thick beryllium window) operating at 40 KeV and 0.25 mA for 25 minutes. The corresponding emission peak is 24 keV [16], which was used to calculated linear attenuation coefficients of enamel mineral (using density of 2.99 gcm^{-3}) [17] and aluminum (using density of 2.7 gcm^{-3}) as described previously [11]. Developed radiograph plates were photographed in a transmitted light microscope using digital camera (Nikon D80, Japan) in a single session (with standardized illumination conditions) and a number of images (of NEC and aluminum step-wedge, Raw images R, of the field of view without the plate, flat field F, and the field of view with the lens of the camera blocked, dark field D) were obtained to proceed in an image analysis freeware (ImageJ, NIH, USA) the following image processing: (R-D)/(F-D) [18]. This treated heterogeneous illumination of the field of view in order to avoid bias in measuring gray levels. Using a calibration curve

between gray levels and aluminum thickness fitted with a fourth order polynomial (R^2 = 0.999), percent mineral volume (V_1) was measured at the selected histological of the surface layer of NEC from:

$$V_1 = \frac{\mu_{Al} \cdot t_{Al}}{\mu_m \cdot t_s} \cdot 100 \quad (1)$$

Linear attenuation coefficients of aluminum (5.884) and enamel hydroxyapatite (11.445) are μ_{Al} and μ_m, respectively. t_{Al} means the aluminum thickness corresponding to the same gray level measured at a histological location (15 x 15 µm). t_s stands for sample thickness at the same histological point.

The sample size comprised three histological points (in a row, with a separation of 50 µm from one to the next) at the surface layer of each lesion (n = 63). All subsequent measurements of component volumes were performed at the same locations.

2.3 Quantification of water and organic volumes and the loosely bound water (permeability)

Birefringence at the selected histological points under water immersion (24 h of immersion) were measured (mean of five measurements) with a Berek compensator in a polarizing microscope (Axioskop 40, Carls Zeiss, Germany) equipped with a green filter (546 nm, bandwidth of 10 nm; Edmund Optics, USA). Observed birefringence (BR_{obs}) in water was interpreted using the approach of Sousa et al. [19] in order to quantify water (α) and organic (β) volumes. This procedure has been described in details previously [11, 12, 20]. Currently, those calculations are performed by customized software which is freely downloadable through the site (http://hotfile.com/dl/204330734/6099675/EBI-0.1.jar.html). Then, we calculated the water more easily available for diffusion (α_d, which we call a permeability parameter) by [12]:

$$\alpha_d = \frac{\alpha^2}{\alpha + \beta} \cdot 100 \quad (2)$$

This equation is the product of α by α/(100-V_1), representing the effective pore size and the inverse of pore viscosity, respectively.

2.4 Quantification of the infiltration of Thoulet´s solutions

After measuring BR_{obs} in water, each sample was dried at room temperature (25º C and 50% of relative humidity) for 48 hs and then immersed in an aqueous solution with mercuric potassium iodide (Thoulet´s solution; pH between 6 and 7) with refractive index of 1.47. Such solution was prepared with dissolving equal amounts of mercuric and potassium iodide in distilled water until the refractive index (measured in an Abbe refractometer) reached 1.47. Hereafter this solution will be called Thoulet 1.47. After dehydration, each section was immersed in Thoulet 1.47 for 24 h and then birefringence was measured (using a Berek compensator) at the same points analyzed before.

After that, all samples were immersed in water again and the water was changed until the retardation returned to values initially found under water immersion. Then, a new drying procedure and an immersion for 24 h in Thoulet´s solution with refractive index 1.40 were performed in order to measure birefringence in this medium. Thoulet´s 1.4 was prepared in the same way as Thoulet´s 1.47.

One of the main challenges in NEC is that after drying those lesions become opaque (no birefringence) and hence loosely bound water (α_2) cannot be measured directly. It is important to quantify how much air (which replaces α_2 after drying) was replaced by the infiltrating material and whether it replaced or not part of firmly bound water (α_1) found in enamel pores after drying. A recent finding (reported by our group) on the relationship between loosely bound water and organic volume brought a way to calculate an approximation of α_2 from

experimental mineral and organic volumes. Once those data were available in all NEC lesions of this study, our approximate experimental α_2 was given by [21]:

$$\alpha_2^{\exp} = \alpha_2^{theo} - 0.5759 - 0.7396\Delta\beta \quad (3)$$

α_2^{theo} is the predicted α_2 as a function of the experimental mineral volume and its volume *fraction* is calculated by [20]:

$$\alpha_2^{theo} = 0.6987 - 1.2487 \cdot \left(\frac{V_1}{100}\right) + 0.544 \cdot \left(\frac{V_1}{100}\right)^2 \quad (4)$$

And $\Delta\beta$ is the difference between experimental and predicted organic volume. The fraction of the predicted organic volume is given by [20]:

$$\beta_{theo} = 0.08654 + 0.46808 \cdot \left(\frac{V_1}{100}\right) - 0.584 \cdot \left(\frac{V_1}{100}\right)^2 \quad (5)$$

The values found by Eqs. (4-5) have to be multiplied by 100 in order to be inserted in Eq. (3). α_2^{theo} is a parameter inversely related to pore viscosity.

By doing this, we assumed that dried NEC had an air volume equal to $\alpha_2^{\exp}$. Using this value in the mathematical approach for interpretation of BR_{obs} published by Sousa et al [19], it could be possible to quantify the volumes infiltrated by Thoulet's solutions, by air (if any) and by α_1, reasonably approaching to the real situation. The volume of air and α_1 after infiltration of Thoulet 1.47 were different from those quantified after infiltration of Thoulet 1.40.

2.5 Real-time two-dimensional mapping of the infiltration of Thoulet's solutions

Some samples (n =10) were selected to perform a real-time mapping of the infiltration of Thoulet's 1.47 and 1.4 into NEC. An orientation-independent polarizing microscope system with one variable retarder (known as "single polscope") [22] was used to map two-dimensional changes in birefringence during infiltration of dried enamel by Thoulet's solutions. This system measures phase retardation at all points of the sample in the field of view independently of the sample orientation, by rotating the polarization states of light rather than rotating the sample, allowing the exploration of new information on the transport of materials in enamel. Along the light path of the transmitted light microscope, the main components of the system consisted of an interference green filter (546 nm, bandwidth of 10 nm, Edmund Optics, USA), a rotatable linear polarizer, a liquid crystal variable retarder covered with an achromatic quarter-wave retardation film for 544 nm (Meadowlark, USA), the sample (between glass slide and cover glass and immersed in test solution), a 4X pol fluorite objective lens, a second achromatic quarter-wave retardation film for 545 nm (Meadowlark, USA), a second linear polarizer, and a digital camera in monochromatic mode (Nikon D7000, Nikon, Japan). Both quarter wave-films were aligned at + 45º. The liquid crystal generates different polarization states of light when voltage is applied. We used the four-frame algorithm that employs four polarization states in response to four specific applied voltages [22]. Each polarization state was obtained by the following sequence of azimuths of the optic axes of the liquid crystal: 270º, 225º, 180º, and 135º. The voltages used to generate such azimuths were provided by the manufacturer of the liquid crystal. Voltages were applied by a signal generator (model AFG 3021B, Tektronix, USA) using AC voltage with square wave and frequency of 2 kHz. This system is able to quantify retardances up to λ/2 for maximum angle of 90º of the first polarizer. We used an angle of 87º, which allowed measurements of retardances up to 265 nm. The system was calibrated with a sample of normal enamel with points where retardance had been measured with the Berek compensator. A good agreement between single polscope and Berek compensator was achieved.

After drying, the sample was placed between glass slide and cover glass and Thoulet' solution (1.47 or 1.4) was injected with a brush into the space between the cover glass and the glass slide and diffused to the sample. Starting

one minute after the injection of the test solution, a series of measurements of changes in birefringence were performed at the following time intervals: at 1 minute intervals within the first 10 minutes, at 5 minutes intervals up to 1 hour after injection. Technical problems did not allow longer periods. During each series, both the digital camera and the signal generator were controlled by customized software that automatically synchronized (during the whole 1 hour period) the signal generator (to release the proper voltage to the liquid crystal) and the digital camera (to shoot). The four resulting images were treated with the four-frame algorithm provided by Shribak [22], resulting in an image of the map of birefringence in enamel. Changes in retardance (retardance multiplied by sample thickness is the birefringence) were used to map the infiltration of the solutions.

2.6 Data analysis

We calculated the relationship between the proportion of the pore volume infiltrated by each Thoulet's solution and each one of the following parameters: mineral volume, α, β, α_d, and α_2^{theo}. In addition to the main hypothesis of the study, we tested the hypothesis that viscosity of the test material (Thoulet`s 1.47 is more viscous than Thoulet`s 1.40) would be directly proportional to the strengths of the predictions. The magnitudes of the differences between R^2 parameters were tested using Cohen's effect size for proportions [23]:

$$h = \phi_x - \phi_y \qquad (6)$$

and

$$\phi = 2 \cdot \arcsin\sqrt{P} \qquad (7)$$

Where P is the R^2 coefficient between a candidate predictor and the proportion of the pore volume infiltrated by Thoulet's solution, and ϕ_x and ϕ_y are related to R^2 coefficients of α_d and of another parameter (mineral volume, α, β or α_2^{theo}) under comparison, respectively. Real-time 2D mapping of solutions' infiltration was analyzed qualitatively by visual examination.

3 Results

Typical histopathological features of NEC lesions are shown in Fig. 1. Parts of the surface layer (negatively birefringent) and the positively birefringent body of the seen under water immersion (Fig. 1B) are shown as opaque (no birefringence) under air immersion (before infiltration with Thoulet's solution) (Fig. 1C-D). In Thoulet's 1.40, the surface layer was negatively birefringent and the body of the lesion presented a reduced positive birefringent (Fig. 1E). Under immersion in Thoulet's 1.47 the lesion is completely negatively birefringent (Fig. 1F).

Fig. 2 shows the mineral (V_1), organic (β), and total water (α) volumes for all histological points, and the corresponding α_d values are shown in Fig. 3a. For the experiment with Thoulet's 1.40, five lesions could not be analyzed because of some technical problems during handling, yielding a total of 48 points, while all 63 points were included in the experiment with Thoulet's 1.47 (the first one). The volumes infiltrated by Thoulet's 1.40 ($\alpha_2^{1.40}$) and Thoulet's 1.47 ($\alpha_2^{1.47}$), and the firmly water volumes found after 24h immersion in Thoulet's 1.47 ($\alpha_1^{1.47}$) and 1.40 ($\alpha_1^{1.40}$) as shown in Fig. 3b-e. For both solutions, some small volumes remained filled with air at some points (data not shown).

Analysis of all candidate predictors of the proportion of the pore volume infiltrated by Thoulet's 1.47 ($\alpha_2^{1.47}/V_2$) and Thoulet's 1.40 ($\alpha_2^{1.40}/V_2$) showed that best predictor for Thoulet's 1.47 was α_d (R^2 = 0.505), followed (in decreasing sequence) by loosely bound water (α_2^{theo}), α, V_1, and β (Fig. 4). For Thoulet's 1.40,

α_d was again the best predictor, but with a predictive value (R^2 = 0.435) that was lower than that for Thoulet's 1.47; in addition, β had very similar predictive value (R^2 = 0.421). The remaining predictors were (in decreasing sequence): V_1, α_2^{theo}, and α (Fig. 4).

Pair-wised analysis of the magnitude of the differences between predictions of ad and those of all other parameters that, for Thoulet's 1.47, the improved predictive value of α_d ranged from almost moderate (with α and α_2^{theo}) to large (with V_1 and β) (Table 1). For Thoulet's 1.40, the improved predictive value of α_d ranged from negligible (with β), small (with V_1), to large (with α and α_2^{theo}) (Table 1).

Real-time 2D mapping of infiltration resulted in videos with the first 11 frames obtained at 1 minute intervals and the remaining at 5 minutes intervals (total of 21 frames). We show 4 representative videos of typical features in both solutions. Video 1, from a large field of view, shows that penetration of Thoulet's 1.40 started at the original surface of enamel (the one that existed before cutting the tooth) as a unidirectional flow following prisms paths within the main body of the section down to the body of the lesion, where, after reaching its bottom, a new flow of both air and Thoulet's 1.40, now towards the opposing direction (to the enamel surface) but also following prisms paths, was added to the inward flow and contributed to the filling of the lesion. Penetration through the pores at the enamel surfaces exposed after cutting and grinding was negligible. A closer view of the outer layers is shown in video 2, where Thoulet's 1.40 forms very thin cylinders (following prisms paths) that rapidly reach a region of lower permeability at the bottom of the body of the lesion, after which the lesion in filled from both a flow coming from the surface layer and another flow coming from the bottom of region with higher permeability (the body of the lesion). Air bubbles are seen emerging at the original surface of enamel.

Video 3 and 4 show the same lesion during infiltration of Thoulet's 1.47. Video 3 confirms that penetration started at the original enamel surface and was negligible at the other surfaces available. The penetration rate is, however, slower and air bubbles were not seen. Video 4 shows (a closer view) that as Thoulet's 1.47 penetrates, it forms cylinders that are thicker compared to those of Thoulet's

1.40, displacing less air in depth than Thoulet's 1.40 did. The solution takes longer to reach the bottom of the body of the lesion and the late outward flow is less intense compared to Thoulet's 1.40.

4 Discussion

In this study we used Thoulet's solutions, which played an important role in the early analysis of the histological layers of NEC [15], because they do not result in either demineralization or remineralization, allowing subsequent analysis to be performed in a same undisturbed sample. The real-time 2D mapping of infiltration, reported for the first time in the literature, provided unavailable new information for the interpretation of data. Contrary to the most dominant current assumption, penetration of the test solutions was negligible through the cut surfaces of ground sections regardless of the different apparent enamel porosity within the main body of the sections. We provide evidences that the surfaces exposed by the grinding procedure, which comprise more than 90% of the open-pore area exposed to the solutions, give negligible contribution to penetration of such solutions. This is similar to a recently reported phenomenon that occurred when ground sections of normal (sound) enamel were dried at room temperature, consisting of water being displaced towards inner enamel while the preceding points (closer to the enamel surface) were replaced by air, all following prisms paths in the main body of the section [14]. This later report and ours suggest that, in both cases, the main pathways for the transport of materials were prisms sheaths, a system of tubular nanochannels composed by the largest pores of enamel that do not connect each other laterally (in cross section) [8]. If sheaths do not connect each other laterally even in established NEC, probably the enlargement of such sheaths, a natural feature of enamel caries [24] even in the early stages [25], occurs mostly due to an expansion of the sheaths towards the center of the prisms. Pore sizes in the prism core and in interprismatic enamel would be so small that diffusion rate is greatly reduced, so that infiltration was negligible at the time intervals analyzed here. This explanation requires that the nanostrucure of the enamel crystallites are highly

preserved in NEC, a feature that has been recently shown by high resolution 3D X-ray scattering [26].

Qualitatively, the mechanics of the flow of the solutions showed some important differences between them regarding the thickness and the velocity of the penetrating cylinders they formed. Thoulet's 1.40, the less viscous, with thinner and more rapid penetrating cylinders, reached deeper at the bottom of the body of the lesion and subsequent infiltration had a contribution from displacement of both solution and air from the bottom of the body of the lesion to the enamel surface in an extent that was greater than with Thoulet's 1.47. Assuming that such pattern is representative of what happens during all the infiltration time, it is likely that infiltration of Thoulet 1.40 in the surface layer is expected to be disturbed more intensively than infiltration of Thoulet's 1.47. This can explain why infiltration of Thoulet's 1.47 was more efficiently predicted than infiltration of Thoulet's 1.40.

The quantitative volumetric data on the infiltration of a test material in NEC, reported for the first time, shows that most of the pore volume was not infiltrated (Fig. 3). We confirmed our hypothesis that α_d is the best predictor of the proportion of pore volume infiltrated by the test solutions. This supports the proposition that α_d can be as a measure of permeability [12]. Among all parameters, including one that is related to pore viscosity, α_d was shown to be the best predictor of infiltration.

The Einstein equation for diffusion and the models on one-dimensional diffusion predict that diffusion rate increases with pore size and decreases with pore viscosity and the distance to be penetrated by the diffusate [10]. The improved predictive value of α_d can be explained by the fact that it accounts both effective pore size and pore viscosity, while the other parameters are more restrict. The (quasi) experimental loosely bound water volume (α_2^{theo}), for example, accounts for viscosity only. Considering the different viscosities of the Thoulet's solutions, previous evidences of a lower diffusion rate of concentrated salt solutions in internal histological points of normal [27] and developing enamel [20], and theoretical diffusion models [10], it was expected (and was confirmed by our 2D mapping) that Thoulet's 1.40 would diffuse faster. In this context, we hypothesized that prediction of infiltration would be better for Thoulet's 1.40, but

this was rejected. The reason why α_d and β had similar predicted values with regard to Thoulet's 1.40 cannot be explained by our results and needs further investigation, but it is probably related to the lower viscosity of such solution. Our interpretation is that the mechanics of the flow of the infiltrant must be taken into account to get a deeper insight into the nature of the transport of materials in NEC. Mineral volume was a very poor predictor of infiltration of Thoulet's 1.47, but was a relatively moderate predictor value for Thoulet's 1.40 (Fig. 4f). Considering that resin infiltrants' viscosity is more similar to Thoulet's 1.47 than to Thoulet´s 1.40, our data is not in line (at least at first analysis) with the report that a more porous surface layer improves resin infiltration into NEC [7]. It might be possible that demineralization results in better infiltration of less viscous material (Fig. 4f). Our data indicate that removal of organic matter increases permeability, giving support for the improved infiltration of calcium ions into NEC after deproteinization [5].

The single polscope proved to be a valuable tool to study the infiltration of Thoulet's solutions, opening new avenues for what might be a new scope of investigation: flow mechanics in enamel. Knowledge on this subject might provide more sophisticated mechanistic explanations for the transport of materials in NEC, which is one of the very basic points underpinning improvements in remineralization and resin infiltration of enamel caries. As passive diffusion is the main mechanism of transport of materials in enamel in vivo [8, 9], our data show that in vitro studies with ground sections might provide information that resembles the in vivo situation more closely than previously thought.

In conclusion, we confirmed our hypothesis that α_d is the best predictor of the proportion of pore volume infiltrated by Thoulet's solutions. Real-time 2D mapping of infiltration indicated that this later occurs mostly along prisms sheaths and unidirectionally in the main body of ground sections of NEC. Data on effective pore volume, pore viscosity and from fluid flow mechanics provided unprecedented information on the nature of the infiltration of materials in the surface layer of NEC.

Acknowledgements

The authors would like to thank the great help given by Dr Michael Shribak (Marine Biological Laboratory, USA) in the selection of the appropriate parts of the single polscope to be acquired and in the alignment of those parts in single polscope setup. The invaluable help of Mr. Yuri Gonzaga (master in computer science, Federal University of Paraiba, Brazil), who developed the softwares used to control the single polscope and obtain retardance images, is greatly acknowledged. The first two authors of this study were financially support by scholarships from CNPq (Brazilian Ministry of Science, Technology and Innovation).

Disclosures

Authors declare no conflicts of interests.

References

[1] Cochrane NJ, Cai F, Huq NL, Burrow MF, Reynolds EC. New approaches to enhanced remineralization of tooth enamel. J Dent Res 2010; 89:1187-1197.

[2] Paris S, Meyer-Lueckel H. Infiltrants inhibit pregression of natural caries lesions *in vitro*. J dent Res 2010; 89: 1276-1280.

[3] Meyer-Lueckel H, Paris S, Kielbassa AM. Surface layer erosion of natural caries lesions with phosphoric and hydrochloric acid gels in preparation for resin infiltration. Caries Res 2007; 41:223-230.

[4] Meyer-Lueckel H, Paris S. Infiltration of natural caries lesions with experimental resins differing in penetration coefficients and ethanol addition. Caries Res 2010; 44:408-144.

[5] Robinson C, Hallsworth AS, Shore RC, Kirkham J. Effect of surface zone deproteinisation on the access of mineral ions into subsurface carious lesions of human enamel. Caries Res 1990; 24:226-230.

[6] Cochrane NJ, Andreson P, Davis GR, Adams GG, Stacey MA, Reynolds EC. An x-ray microtomographic study of natural white-spot enamel lesions. J Dent Res 2012; 91:185-191.

[7] Neuhaus KW, Schlafer S, Lussi A, Nyvad B. Infiltration of natural caries lesions in relation to their activity status and acid pretreatment *in vitro*. Caries Res 2013; 47:203-210.

[8] Shellis RP, Dibdin GH. Enamel microporosity and its functional implications; in: Teafor MF, Smith MM, Fergunson MWJ (eds): Development, function and evolution of teeth. New York: Cambridge University Press, 2000,pp. 242-251.

[9] Shellis RP. Transport processes in enamel and dentin, in book on Tooth wear and sensitivity; in: Addy M, Embery G, Edgar WM, Orchardson R (eds): Tooth wear and sensitivy. London: Martin Dunitz, 2000, pp. 19-28.

[10] Dusenbury DB. Living at Micro Scale. Cambridge, Harvard University Press, 2009.

[11] Medeiros RC, Soares JD, Sousa FB. Natural enamel caries in polarized light microscopy: differences in histopathological features derived from a qualitative versus a quantitative approach to interpret enamel birefringence. J Microsc 2012; 246:177-189.

[12] Barbosa de Sousa F, Dias Soares J, Sampaio Vianna S. Natural enamel caries: a comparative histological study on biochemical volumes. Caries Res 2013; 47:183-192.

[13] Dibdin GH. The water in human dental enamel and diffusional exchange measured by clearance of tritiated water from enamel slabs of varying thickness. Caries Res 1993; 27:81-86.

[14] Medeiros RCG, DE Lima TAS, Gouveia CR, Sousa FB. Water loss at normal enamel histological points during air drying at room temperature. J Microsc 2013; 250:218-227.

[15] Darling AI, Studies of the early lesion of enamel caries. Br Dent J 1958; 105:119-135.

[16] Boone JM, Fewell TR, Jennings RJ. Molybdenium, rhodium, and tungsten anode spectral modes using interpolating polynomials with application to mammography. Med Phys 1997; 24: 1863–1874

[17] Elliott JC. Structure, crystal chemistry and density of enamel apatites. In: Chadwick D, Cardew G (eds). Dental enamel, Ciba Foundation Symposium 205. Chichester; Wiley; 1997. pp. 54–72.

[18] Murphy DB. Fundamentals of Light Microscopy and Digital Imaging. New York; Wiley-Liss; 2001. p. 43–59

[19] Sousa FB, Vianna SS, Santos-Magalhães NS. A new approach for improving the birefringence analysis of dental enamel mineral content from polarizing microscopy. J Microsc. 2006; 221: 79-83

[20] Sousa FB, Vianna SS, Santos-Magalhães NS. Dental enamel birefringence for a wide mineral content range and for different immersion media's refractive indexes: an improved mathematical interpretation. J Microsc 2009; 23: 69-75

[21] Macena MS, Leite MLA, Gouveia CL, DE Lima TAS, Athayde PA, Sousa FB. A comparative study on component volumes from outer to inner dental enamel in relation to enamel tufts. Arch Oral Biol 2014 (Submitted).

[22] Shirbak M. Complete polarization state generator with one variable retarder and its application for fast and sensitive measuring of two dimensional birefringence distribution. J Opt Soc Am A 2011; 28: 410-419.

[23] Cohen J: A power primer. Psychol Bull. 1992; 112: 155–159.

[24] Orams HJ, Phakey PP, Rachinger WA, Zybert JJ. Ultrastructural changes in the translucent and dark zones of early enamel caries. J Oral Pathol. 1980; 9:54–61

[25] Shellis RP. Scanning electron-microscopic study of solubility variations in human enamel and dentine. Archs Oral Biol 1996; 41:473-484.

[26] Deyhle H, White SN, Bunk O, Beckmann F, Müller B. Nanostructure of the carious tooth enamel lesion. Acta Biomater 2014; 10: 355-364.

[27] Houwink B. The limited usefulness of Thoulet's solution in imbibitions experiments in dental enamel. Br Dent J 1969; 126: 447-450.

Captions for figures and videos

Fig. 1. Typical features of a NEC lesion. A, microradiography showing a surface layer with relatively high gray. B, under polarizing microscopy with Red I retardance filter (which results in red background) and the sample prisms oriented at - 45°, water immersion shows the surface layer (SL) as negatively birefringent and outlining a positively birefringent body of the lesion. C, air immersion clearly shows opaque (no birefringence) enamel at both the surface layer (some parts) and the positively birefringent body of the lesion. D, without Red I filter, background assumes the same color of the opaque parts, making it impossible (from this single image) to distinguish between opaqueness and pseudo-isotropy (when the sample has the same color of the background). E, in Thoulet's 1.40 showing the negatively birefringent surface layer and a reduced positively birefringent body of the lesion. F, under immersion in Thoulet's 1.47 showing the lesion completely negatively birefringent. Scale bars = 500 µm.

Fig. 2. Mineral (V_1), organic (β), and total water (α) volumes for all histological points (n = 63).

Fig. 3. α_d (a), volumes infiltrated by Thoulet's 1.47 ($\alpha_2^{1.47}$, "b") and Thoulet's 1.40 ($\alpha_2^{1.40}$, "d") and the firmly bound water volumes after 24h of infiltration of Thoulet's 1.47 ($\alpha_1^{1.47}$, "c") and Thoulet's 1.40 ($\alpha_1^{1.40}$, "e").

Fig. 4. Linear correlations between possible predictors and the proportion of the pore volume infiltrated by Thoulet's 1.47 ($\alpha_2^{1.47}/V_2$) and Thoulet's 1.40 ($\alpha_2^{1.40}/V_2$). a-d: data on Thoulet's 1.47 showing α_d as the best predicted (R^2 = 0.505). e-h: data on Thoulet's 1.40 showing α_d as the best predictor (R^2 = 0.435) closely followed by β (R^2 = 0.421). α_2^{theo} was a poor predictor for Thoulet's 1.40 ("i"), but the second best for Thoulet's 1.47 ("j").

Video 1. Real-time 2D mapping of the infiltration of Thoulet's 1.40 in a NEC lesion. Total of 21 frames, with the first 11 frames obtained at 1 minute intervals and the remaining at 5 minutes intervals. The penetration of Thoulet's 1.40 started at the original surface of enamel (the one that existed before cutting the tooth) as a unidirectional flow following prisms paths within the main body of the section down to the body of the lesion, where, after reaching its bottom, a new flow of both air and Thoulet's 1.40, now towards the opposing direction (to the enamel surface) but also following prisms paths, was added to the inward flow and contributed to the filling of the lesion. Air bubbles emerge at the original enamel surface. Penetration through the pores at the enamel surfaces exposed after cutting and grinding was negligible. Scale bar = 200 µm.

Video 2. Real-time 2D mapping of the infiltration of Thoulet's 1.40 in a NEC lesion. Same as shown in video 1, but with a closer view of the outer layers. Thoulet's 1.40 forms very thin cylinders (following prisms paths) that rapidly reach a region of lower permeability at the bottom of the body of the lesion, after which the lesion in filled from both a flow coming from the surface layer and another flow coming from the bottom of region with higher permeability (the body of the lesion). Air bubbles are seen emerging at the original surface of enamel. Scale bar = 100 µm.

Video 3. Real-time 2D mapping of the infiltration of Thoulet's 1.47 in the same NEC lesion shown in videos 1 and 2, using the same time intervals. It shows that penetration started at the original enamel surface and was negligible at the other surfaces available. The penetration rate is, however, slower and air bubbles were not seen. Scale bar = 200 µm.

Video 4. Real-time 2D mapping of the infiltration of Thoulet's 1.47 in the same NEC lesion shown in videos 1 and 2. Same as shown in video 1, but with a closer view of the outer layers. As Thoulet's 1.47 penetrates, it forms cylinders that are thicker compared to those of Thoulet's 1.40, displacing less air in depth than Thoulet's 1.40 did. The solution takes longer to reach the bottom of the body of the lesion and the late outward flow is less intense compared to Thoulet's 1.40. Scale bar = 100 µm.

Figure 1

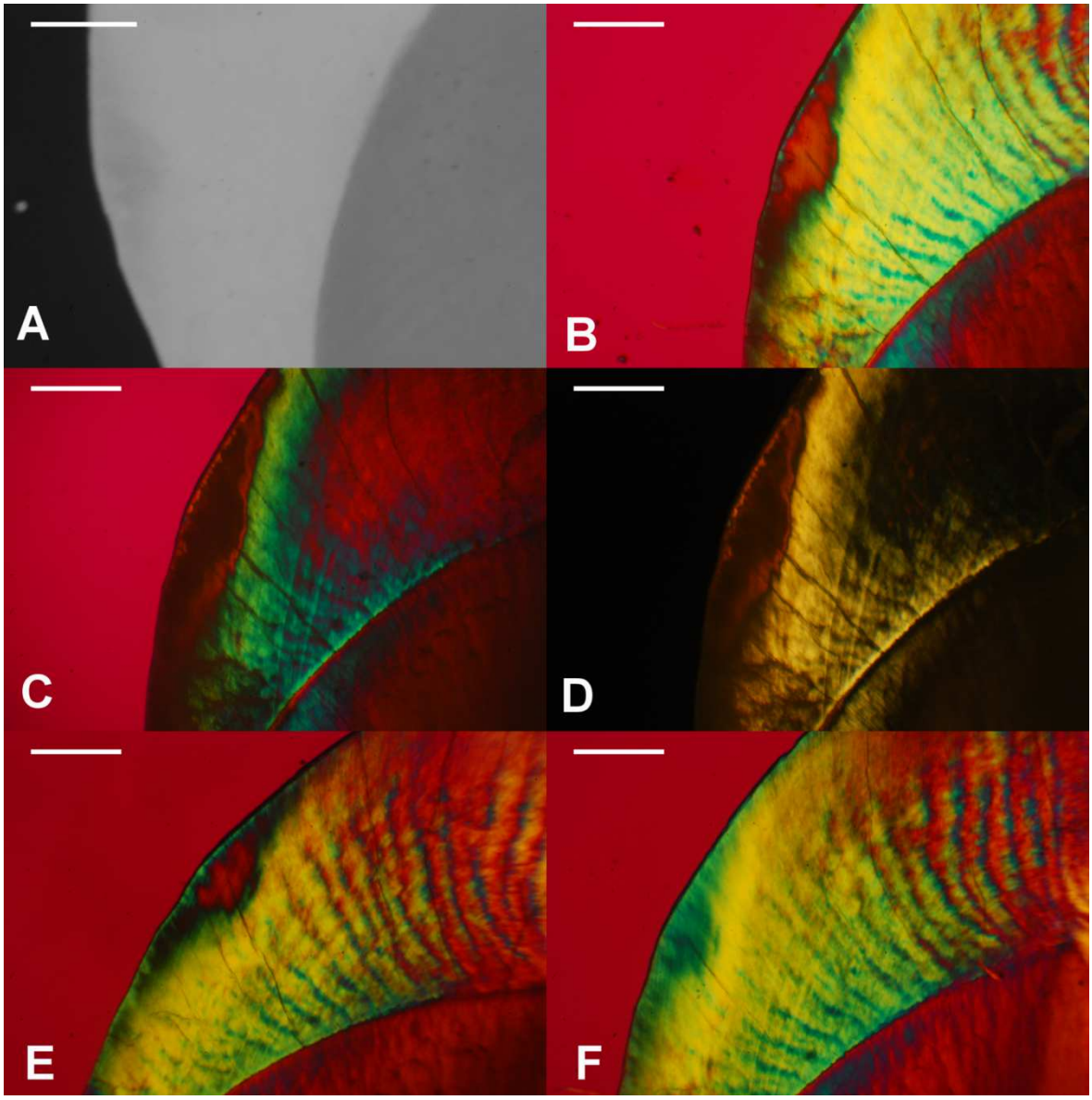

Figure 2

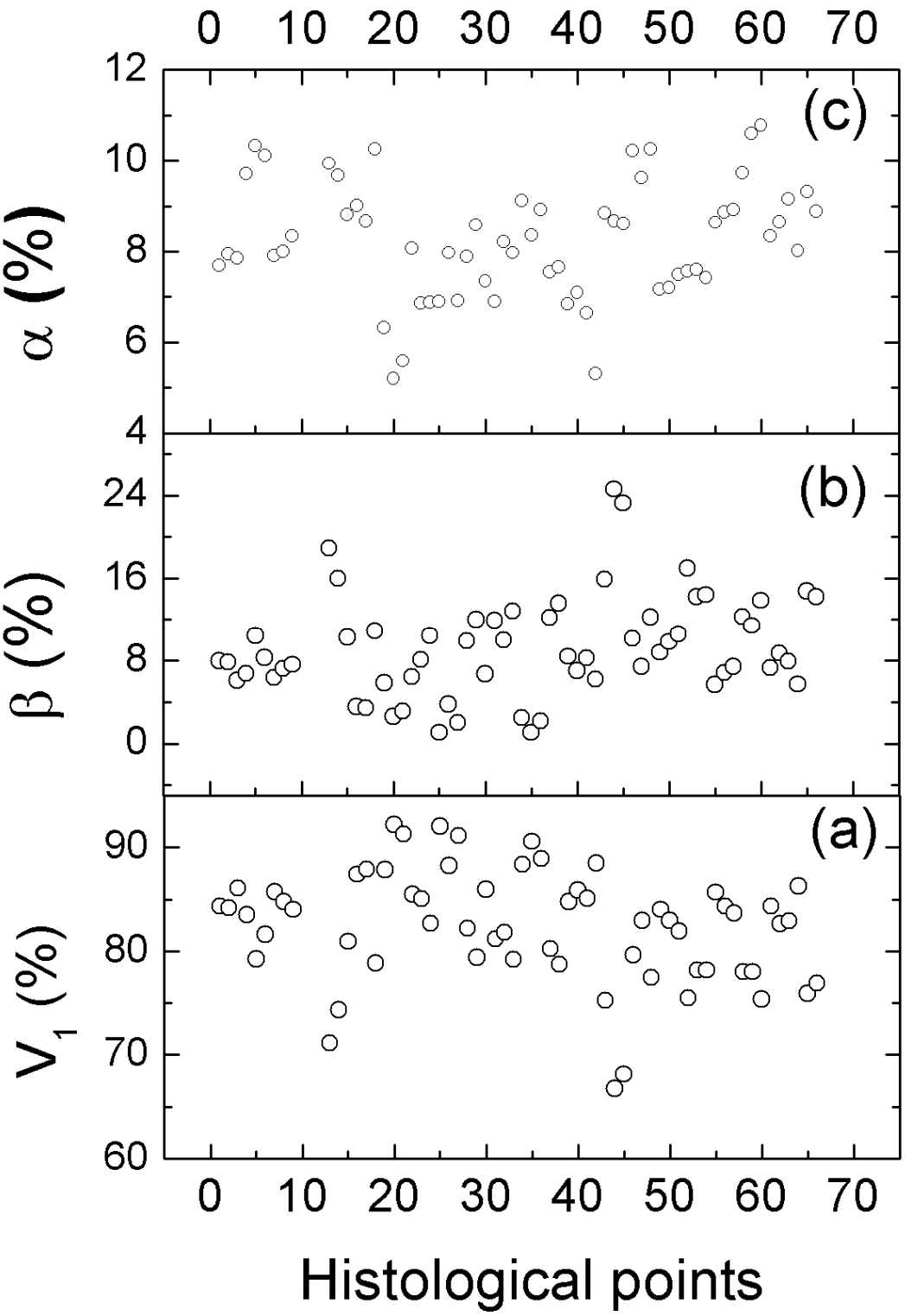
0 10 20 30 40 50 60 70
12
10
8
6
4
α (%)
(c)
24
16
8
0
β (%)
(b)
90
80
70
60
V1 (%)
(a)
0 10 20 30 40 50 60 70
Histological points

Figure 3

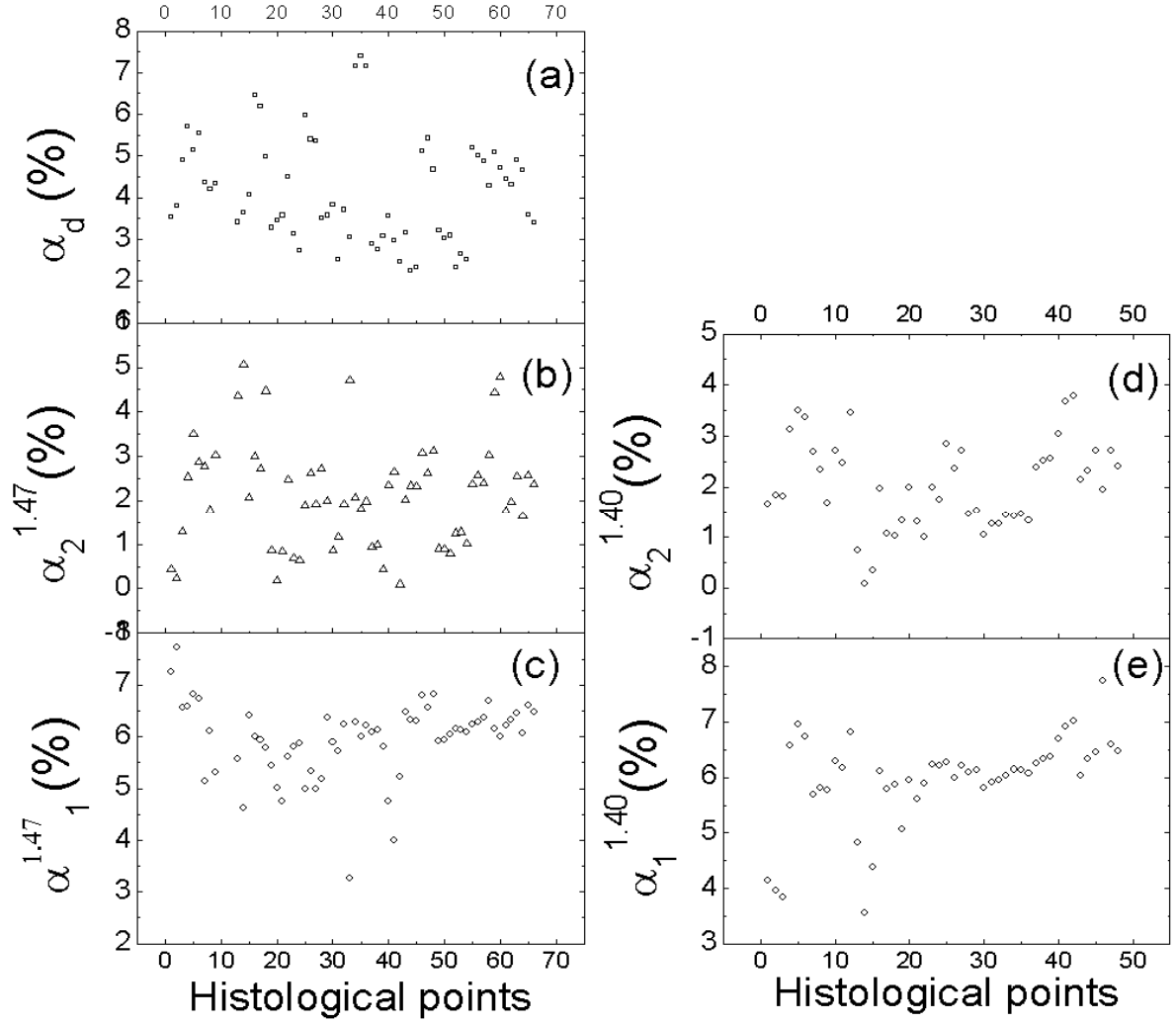
(a)
(b)
(c)
(d)
(e)
α_d (%)
$\alpha_2^{1.47}$(%)
$\alpha_1^{1.47}$(%)
$\alpha_2^{1.40}$(%)
$\alpha_1^{1.40}$(%)
Histological points
Histological points

Figure 4

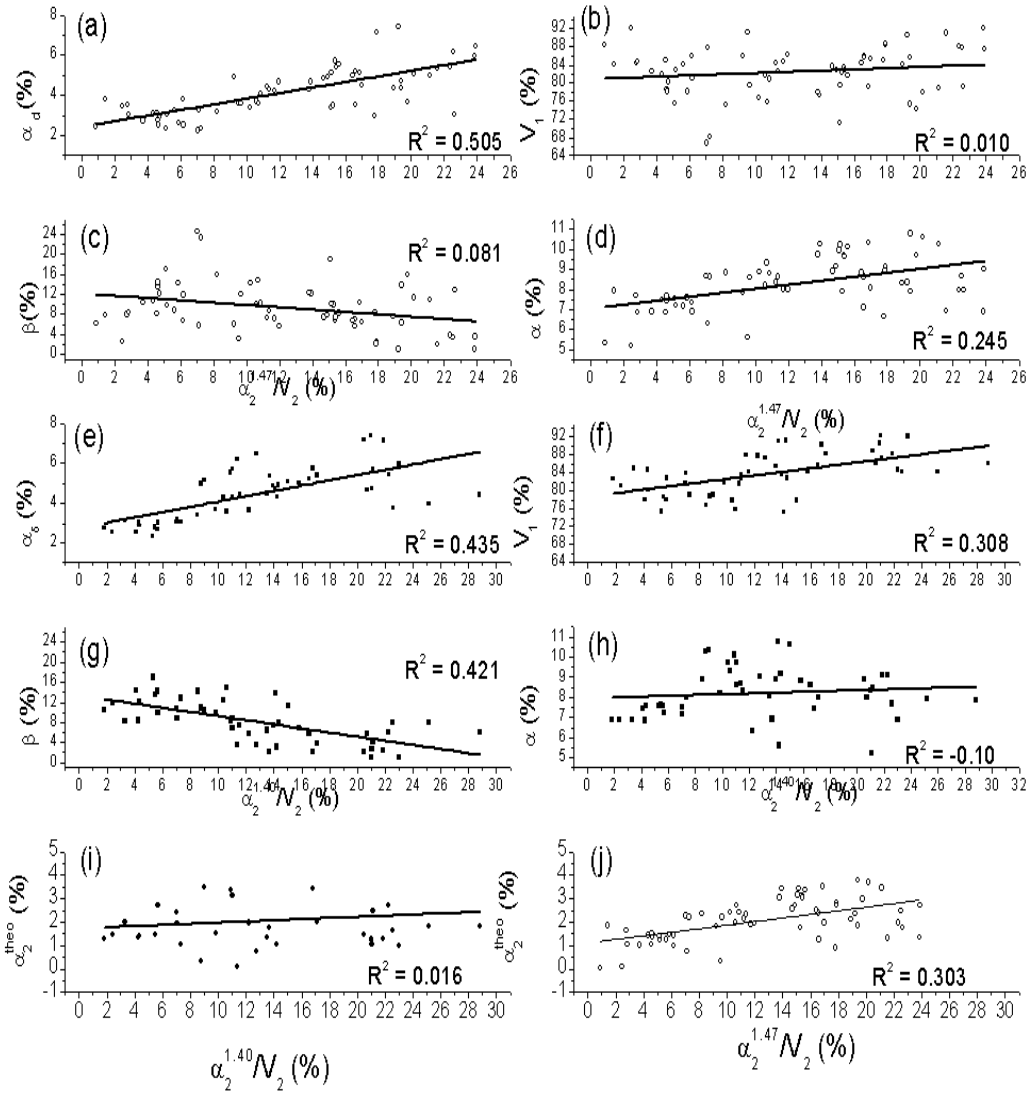
(a)
α_d (%)
R^2 = 0.505
(b)
V_1 (%)
R^2 = 0.010
(c)
β(%)
R^2 = 0.081
$\alpha_2^{1.47}/V_2$ (%)
(d)
α (%)
R^2 = 0.245
(e)
α_δ (%)
R^2 = 0.435
(f)
V_1 (%)
R^2 = 0.308
(g)
β (%)
R^2 = 0.421
$\alpha_2^{1.44}/V_2$ (%)
(h)
α (%)
R^2 = -0.10
$\alpha_2^{1.40}/V_2$ (%)
(i)
α_2^{theo} (%)
R^2 = 0.016
$\alpha_2^{1.40}/V_2$ (%)
(j)
α_2^{theo} (%)
R^2 = 0.303
$\alpha_2^{1.47}/V_2$ (%)

Table 1

Table 1. Effect sizes* for pair-wise comparisons between a_d and other parameters with regard to the predictive values R^2.

INFILTRANT	***PARAMETERS***			
	V_1	b	a	α_2^{theo}
Thoulet's 1.47				
a_d	1.38	1.00	0.545	0.415
Thoulet's 1.40				
a_d	0.264	0.028	0.797	1.187

*Effect sizes categories [Cohen, 1992]: 0-0.2 is negligible; < 0.5 is small; < 0.8 is moderate; and ≥ 0.8 is large.

Video 1

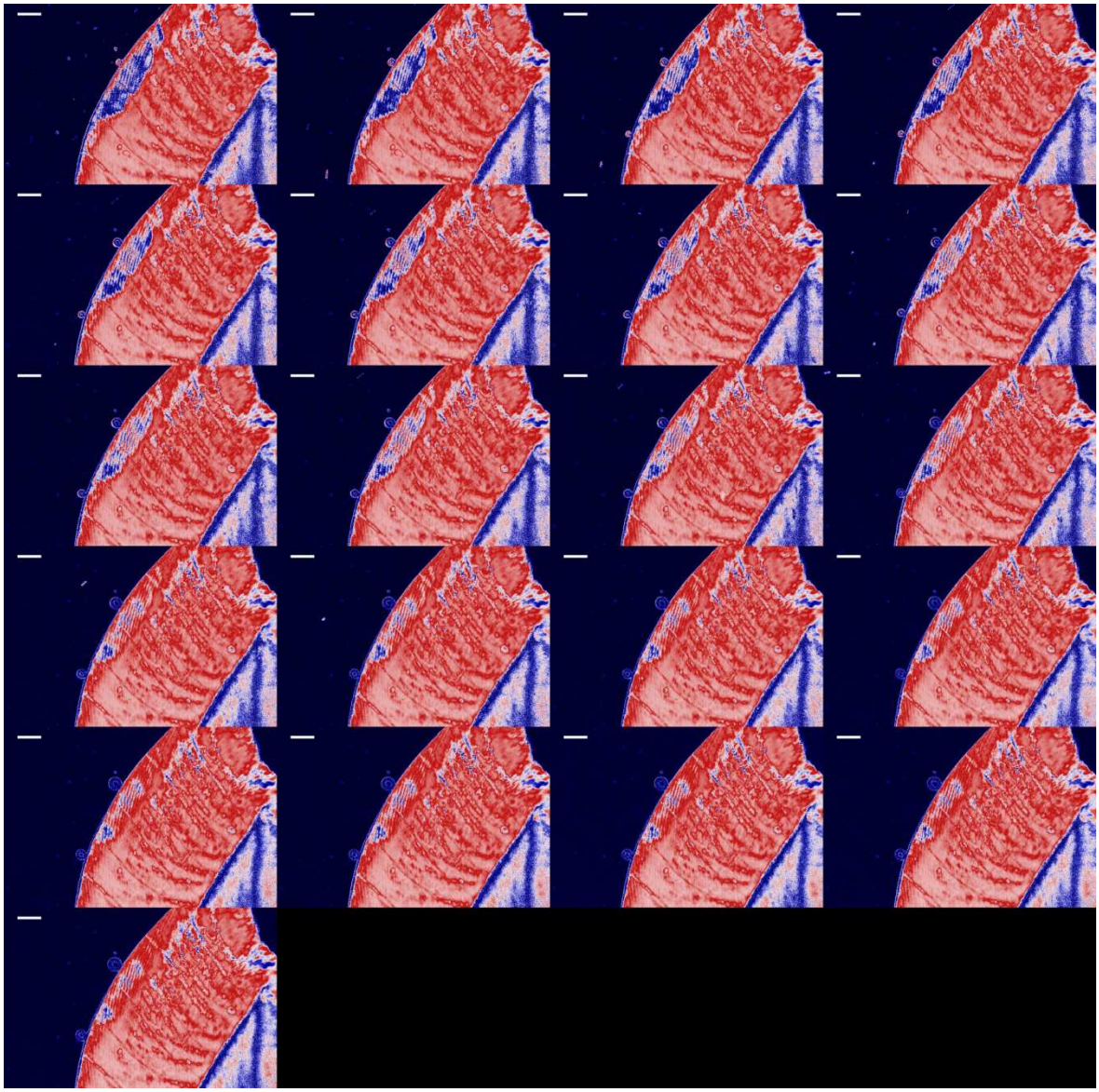

Video 2

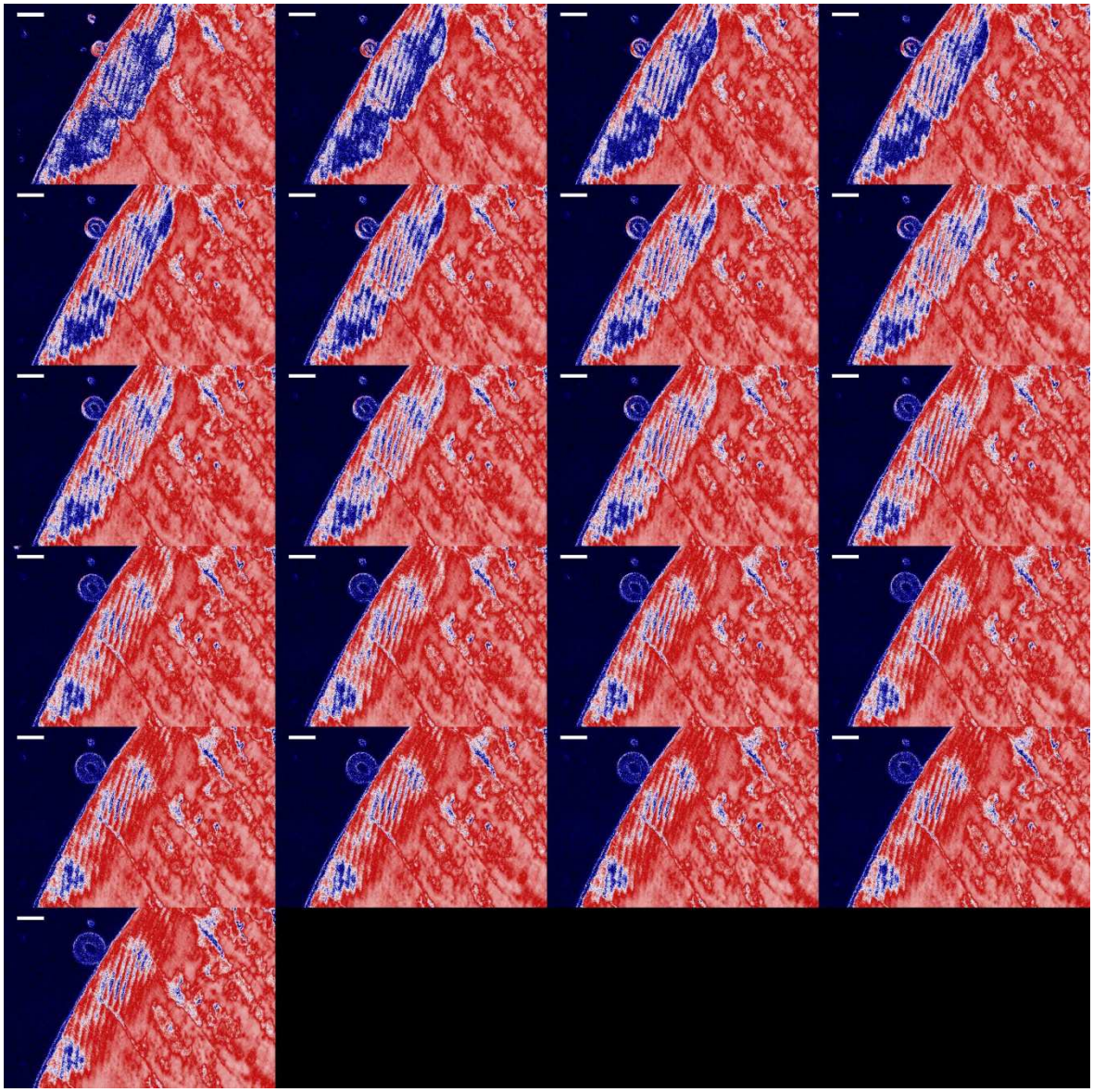

Video 3

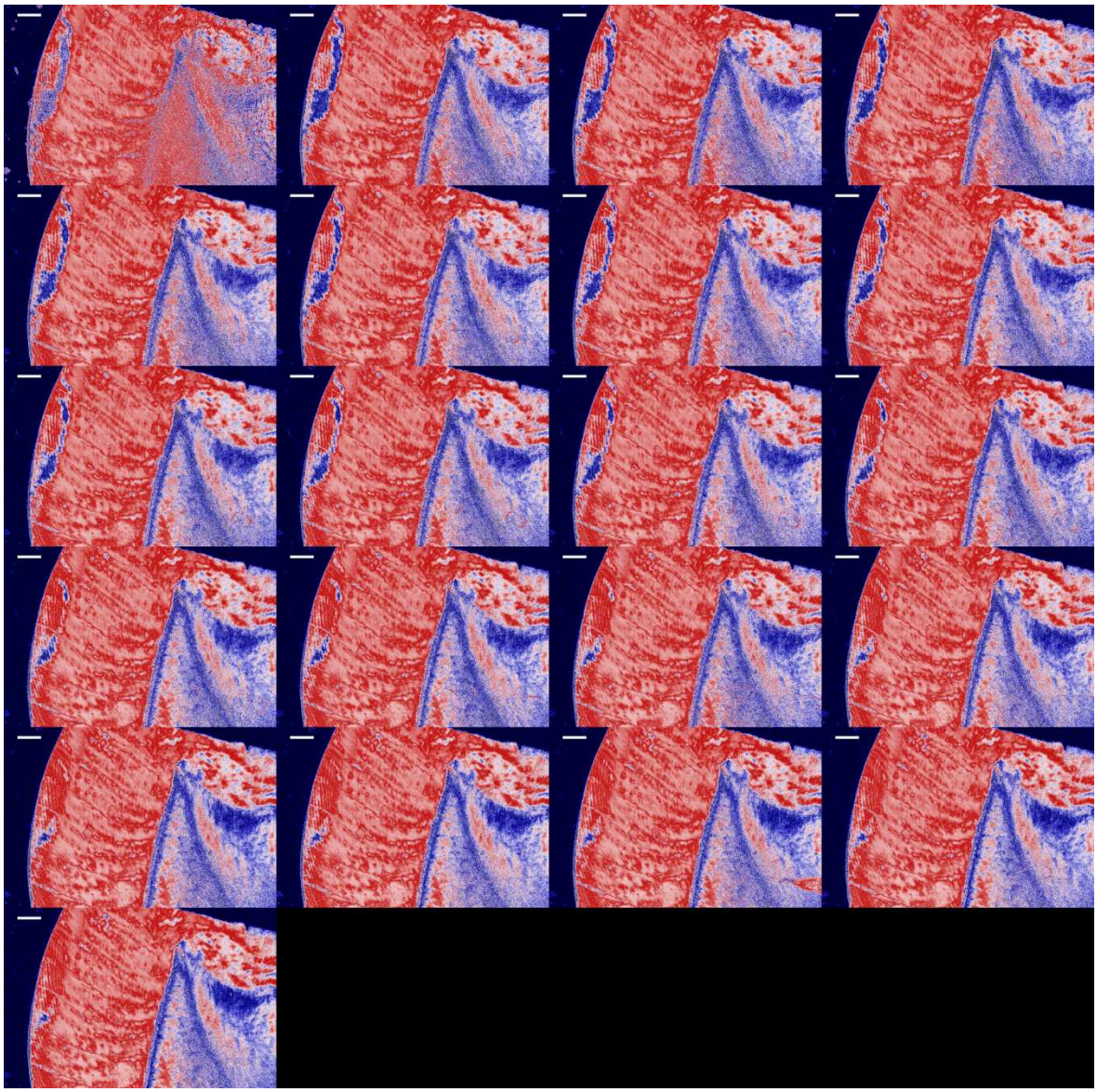

Video 4

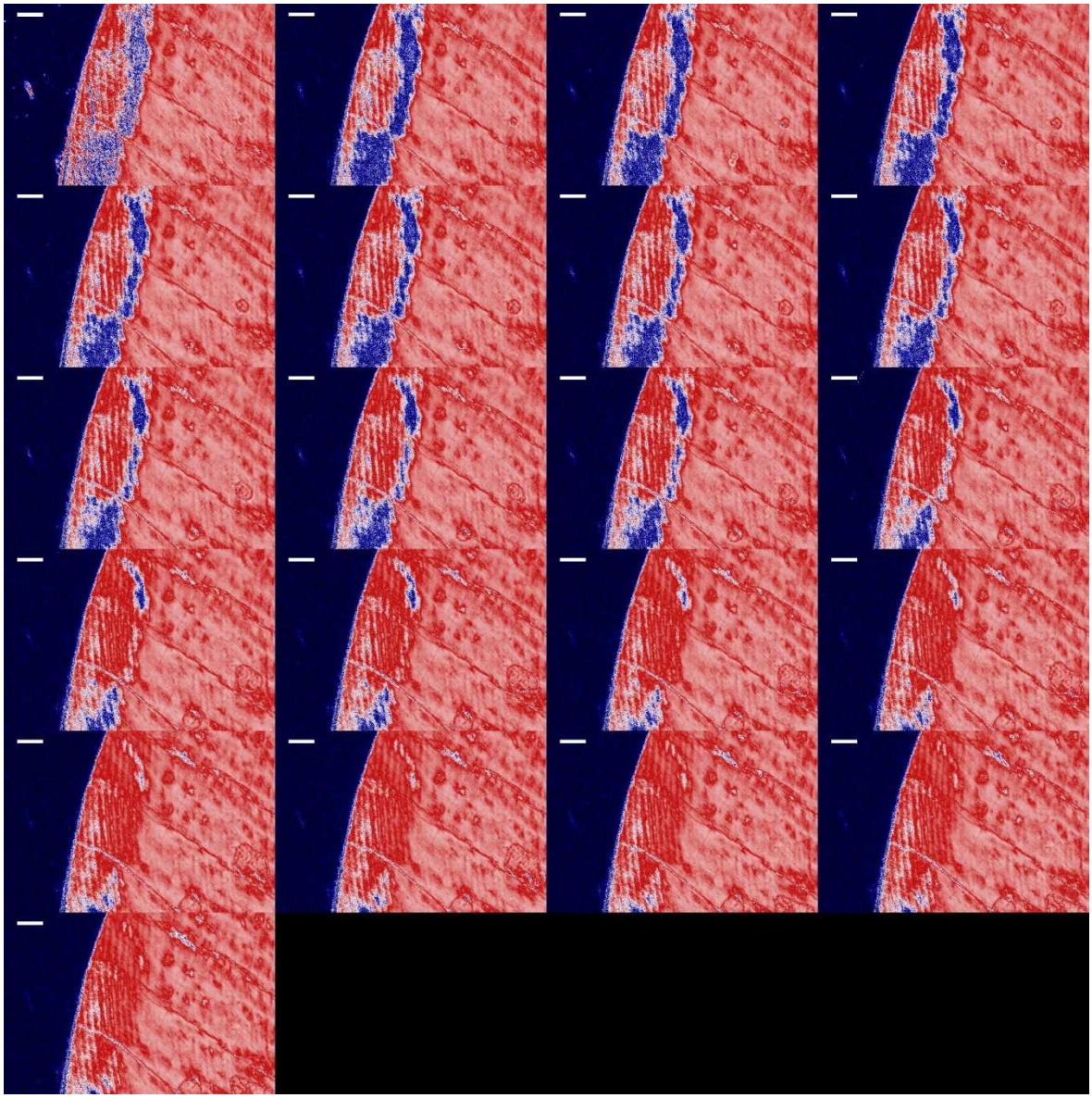

3. CONSIDERAÇÕES GERAIS

Neste estudo foram utilizadas as soluções de Thoulet 1,4 e 1,47, que desempenharam um papel importante na análise inicial das camadas histológicas de lesões cariosas naturais de esmalte[10], pois elas não resultaram em qualquer desmineralização ou remineralização, permitiram análises subseqüentes na mesma amostra sem que a mesma sofresse alterações. O mapeamento 2D de infiltração em tempo real, relatou pela primeira vez na literatura novas informações para a interpretação dos dados. Ao contrário da hipótese mais aceita, a penetração da solução teste foi insignificante através da superfície do corte por desgaste, independente dos níveis de porosidade do esmalte. Fornecemos evidências de que as superfícies expostas ao processo de desgaste, as quais compreendem uma área de 90% de poros abertos expostos às soluções, dão contribuição insignificante à penetração de tais soluções. Isto é semelhante a um fenômeno recentemente relatado quando secções de esmalte normal (sadio) foram desidratadas em temperatura ambiente, a água se deslocou para o interior do esmalte, enquanto que os pontos mais próximos a superfície do esmalte foram substituídos por ar, seguindo a trajetória dos prismas[20]. Esse último relato e o nosso sugere que, em ambos os casos, as principais vias para o transporte de materiais foram as bainhas dos primas, um sistema tubular de nanocanais composta por poros maiores de esmalte que não se conectam lateralmente uns com os outros (em corte transversal)[29]. Se as bainhas não se conectam lateralmente umas com as outras como demonstrado em lesões cariosas naturais de esmalte, provavelmente o alargamento de tais bainhas é uma característica natural da cárie de esmalte[25], mesmo nas fases inicias[30], ocorre principalmente devido a uma expansão das bainhas em direção ao centro dos prismas. As dimensões dos poros no centro do prisma e no esmalte interprismático seria tão pequena que a taxa de difusão é muito reduzida, de modo que a infiltração insignificante para os intervalos de tempos analisados. Esta explicação requer que a nanoestrutura dos cristalitos de esmalte é altamente conservada nas lesões cariosas naturais de esmalte.

Qualitativamente, a mecânica do fluxo das soluções mostrou algumas diferenças importantes dentre eles no que diz respeito a espessura e dos cilindros penetrantes que eles formam. A solução de Thoulet 1,4 é menos viscosa, com cilindros mais finos e a penetração é mais rápida, atingindo mais profundamente na parte inferior do corpo da lesão e a infiltração subseqüente teve uma contribuição no deslocamento de ambos, das soluções e do ar, desde a superfície até o inferior do corpo da lesão numa extensão que foi maior do que com Thoulet 1,47. Assumindo que, tal padrão é representativo do que acontece durante todo o tempo de infiltração, é provável que infiltração de Thoulet 1,40 na camada superficial seja mais intensamente alterada do que a de Thoulet 1,47. Isso pode explicar porque a infiltração de Thoulet 1,47 foi mais eficientemente prevista do que a infiltração por Thoulet 1,40.

Os dados quantitativos volumétricos da infiltração da lesão cariosa natural de esmalte relatam pela primeira vez, que a maior parte dos volumes dos poros não foi infiltrado. Confirmamos nossa hipótese que α_d é o melhor preditor da proporção dos volumes dos poros infiltrados por soluções teste. Isso apóia a proposição de que α_d pode ser uma medida de permeabilidade[2]. Entre todos os parâmetros, incluindo o que se diz respeito à viscosidade dos poros, α_d mostrou ser o melhor preditor de infiltração.

A equação de difusão de Einstein e os modelos de difusão unidimensional prever que a taxa de difusão aumenta com o tamanho dos poros e diminui com a viscosidade dos poros e a distância a ser penetrada pela substância difundida[13]. O valor preditivo melhorado de α_d pode ser explicado pelo fato de que é responsável tanto pelo tamanho efetivo e viscosidade dos poros, enquanto que os outros parâmetros são mais restritos. O volume experimental de água fracamente aderida (α_2^{theo}), por exemplo, considera apenas a viscosidade. Considerando as diferentes viscosidades das soluções de Thoulet, evidências anteriores de uma menor taxa de difusão em soluções concentradas de sais em pontos histológicos mais internos no esmalte normal[17] e em desenvolvimento[35], e em modelos teóricos de difusão[13], esperava-se (e foi confirmado pelo nosso mapeamento 2D) que a solução de Thoulet 1,40 se difundiria mais rápido. Nesse contexto, a hipótese seria de que a previsão de infiltração por Thoulet 1,40 seria melhor, mas essa hipótese foi rejeitada. A razão pela qual α_d e β tiveram valores semelhantes

no que diz respeito ao Thoulet 1,40 não pode ser explicada pelos nossos resultados e precisa de mais investigações, mas é provável que esteja relacionado com a viscosidade dessa solução ser mais baixa. Nossa interpretação é que a mecânica do fluxo do infiltrante deve ser levada em conta para obter um conhecimento mais profundo da natureza do transporte de materiais em lesões cariosas naturais de esmalte. O volume mineral foi um preditor muito insignificante para infiltração de Thoulet 1,47, mas teve uma valor preditivo relativamente moderado em relação a Thoulet 1,40. Considerando que a viscosidade de resinas infiltrantes é mais semelhante ao Thoulet 1,47 do que em Thoulet 1,40, nossos dados não são lineares (pelo menos numa primeira análise) com relatos de que uma camada superficial mais porosa melhora a infiltração por resinas em lesões cariosas naturais de esmalte[24]. Pode ser possível que a desmineralização resulte em uma melhor infiltração de material menos viscoso. Nossos dados indicam que a remoção de matéria orgânica aumenta a permeabilidade, dando suporte para a melhoria da infiltração de íons de cálcio em lesões cariosas naturais de esmalte após desproteinização[27].

A “single Polscope” provou ser uma ferramenta valiosa para estudar a infiltração de soluções da Thoulet, abrindo novos caminhos para o que poderia ser um novo âmbito de investigação: mecânica dos fluidos em esmalte. Conhecimento sobre o assunto pode fornecer explicações de mecanismos mais sofisticadas para o transporte de materiais em lesões cariosas naturais de esmalte, que é um dos pontos muito básicos que sustentam as melhorias na remineralização e infiltração de resina em cárie de esmalte. Como a difusão passiva é o principal mecanismo de materiais em esmalte *in vivo* [29,31], os nossos dados mostram que os estudos *in vitro* com cortes por desgaste podem oferecem informações que se assemelha *in vivo* com mais proximidade do que se pensava anteriormente.

4. CONCLUSÃO

Em conclusão, confirmamos nossa hipótese de que α_d é o melhor preditor da proporção de volume de poros infiltrado por soluções da Thoulet. O mapeamento 2D de infiltração em tempo real indicou que a penetração da solução ocorre principalmente através da superfície do esmalte seguindo em direção ao corpo da lesão pelas bainhas dos prismas. Os dados sobre volume de poros efetivos, da viscosidade dos poros e da mecânica do fluxo do fluido fornecido forneceram informações nunca vistas na literatura sobre a natureza da infiltração de materiais na camada superficial e lesão cariosa natural de esmalte. Nossos estudos podem fornecer uma visão mais profunda sobre o transporte de agentes usados para a remineralização e infiltração de resinas na lesão cariosa natural de esmalte.

REFERÊNCIAS*

1. Atkinson HF. An investigation into the permeability of human enamel using osmotic methods. Brit. Dent. J 1947; 83: 205-214.

2. Barbosa de Sousa F, Dias Soares J, Sampaio Vianna S. Natural enamel caries: a comparative histological study on biochemical volumes. Carie Res 2013; 47(3): 183-192.

3. Bergman G; Lind PO. A quantitative microradiographic study of incipient enamel caries. J Dent Res 1966; 45: 1477-1484.

4. Berkovits BKB, Holland GR, Moxham BJ. Microscopic anatomy of oro-dental tissues: Color Atlas and Textbook of Oral Anatomy, Histology and Embryology, 2 ed. Londres: Mosby Year Book; 1992.

5. Carlstrom D, Glas JE, Angmar B. Studies on the ultrastructure of dental enamel. V. The state of water in human enamel. J. Ultrastruct. Res. 1963; 8(1-2): 24-29.

6. Cochrane NJ, Andreson P, Davis GR, Adams GG, Stacey MA, Reynolds EC. An x-ray microtomographic study of natural white-spot enamel lesions. J Dent Res 2012; 91:185-91.

7. Cochrane NJ, Cai F, Huq NL, Burrow MF, Reynolds EC. An X-ray microtomographic study of natural white-spot enamel lesions. J Dent Res 2012; 91: 185-191.

8. Cochrane NJ, Cai F, Huq NL, Burrow MF, Reynolds EC. New approaches to enhanced remineralization of tooth enamel. J. Dent Res. 2010; 89(11):1187-97.

9. Darling AI. Studies of the early lesion of enamel caries of transmitted light, polarisad light and radiography. . Br Dent J 1956; 101: 289-297.

10. Darling AI. Studies of the early lesion of enamel caries. Br. Dent. J 1958; 105: 119–135

11. Darling AI. The selective attack of caries on the dental enamel.Ann R Coll Surg Enge 1961; 29: 354-369.

12. Dibdin GH. The water in human dental enamel and diffusional exchange measured by clearance of tritiated water from enamel slabs of varying thickness. Caries Res 1993; 27(2): 81-86.

13. Dusenbury DB. Living at micro scale. Cambridge: Harvard University Press; 2009.

14. Dusevich V, Xu C, Wang Y, Walker MP, Gorski JP. Identification of a protein-containing enamel matrix layer which bridges with the dentine-enamel junction of adult human teeth. Arch Oral Biol 2012; 57(12): 1585-1594.

15. He LH, Swain MV. A functionally graded natural coating. Journal of Dentistry 2009; 37: 596-603.

16. He LH, Swain MV. Understanding the mechanical behavior of human enamel from its structural and compositional characteristics. J. Mech Beh of Biomed. Mater 2008; 1(1): 18-29.

17. Houwink B. The limited usefulness of Thoulet's solution in imbibitions experiments in dental enamel. Br Dent J 1969; 126: 447-50

18. Kerebel B, Daculsi G, Kerebel LM. Ultrastructural studies of enamel crystallites. J Dent Res. 1979; 57: 306-312.

19. Margolis HC, Zhang YP, Lee CY, Kent RL, Moreno EC. Kinetics of enamel demineralization in vitro. J Dent Res 1999; 78: 1326-1335.

20. Medeiros RCG, DE Lima TAS, Gouveia CR, Sousa FB. Water loss at normal enamel histological points during air drying at room temperature. J Microsc 2013; 250:218-27.

21. Medeiros RCG, Soares JD, Sousa FB. Natural enamel caries in polarized light microscopy: differences in histopathological features derived from a qualitative versus a quantitative approach to interpret enamel birefringence. Journal of Microscopy 2012; 246(2): 177-189.

22. Meyer-Luckel H, Paris S. Improved Resin Infiltration of Natural Caries Lesions. J Dent Res. 2008; 87(120; 1112-1116.

23. Moreno EC, Zahradnik RT. The pore structure of human dental enamel. Arch Oral Biol. 1973; 18(8): 1063-1068.

24. Neuhaus KW, Schlafer S, Lussi A, Nyvad B. Infiltration of natural caries lesions in relation to their activity status and acid pretreatment *in vitro*. Caries Res 2013; 47:203-10.

25. Orams HJ, Phakey PP, Rachinger WA, Zybert JJ. Ultrastructural changes in the translucent and dark zones of early enamel caries. J Oral Pathol. 1980;9:54–61

26. Pauly S. Permeability and diffusion data. *In*: Branduo J, Immergut EH, Grulker EA, Polymer handbook.4th ed. New York: John Willy and Sons, p.543-569, 1999.

27. Robinson C, Hallsworth AS, Shore RC, Kirkham J. Effect of surface zone deproteinisation on the access of mineral ions into subsurface carious lesions of human enamel. Caries Res 1990; 24:226-30.

28. Sakae T, Suzuki K, Kozawa Y. Tooth Enamel Microstructure: A short review of studies on chemical and physical properties of enamel crystallites. Rotterdam: Balkema; 1997.

29. Shellis RP, Dibdin GH. Enamel microporosity and its functional implications. *In*: Teafor MF, Smith MM, Fergunson MWJ. Development, function and evolution of teeth. New York: Cambridge University Press, p.242-251, 2000.

30. Shellis RP. Scanning electron-microscopic study of solubility variations in human enamel and dentine. Archs Oral Biol 1996; 41(5): 473-484.

31. Shellis RP. Transport processes in enamel and dentin, in book on Tooth wear and sensitivity; in: Addy M, Embery G, Edgar WM, Orchardson R (eds): Tooth wear and sensitivy. London: Martin Dunitz, 2000, pp. 19-28.

32. Silverstone LM. Structure of Carious Enamel, Including the Early Lesion. Oral. Sci. Rev. 1973; 3: 100-160.

33. Silverstone LM. The surface zone in caries and in caries like lesions produced in vitro. Br Dent J. 1968; 125: 145-157.

34. Sousa FB, Vianna SS, Santos-Magalhães NS. A new approach for improving the birefringence analysis of dental enamel mineral content from polarizing microscopy. J. Microsc. 2006; 221(2): 79-83.

35. Sousa FB, Vianna SS, Santos-Magalhães NS. Dental enamel birefringence for a wide mineral content range and for different immersion media's refractive indexes: an improved mathematical interpretation. J Microsc 2009; 23: 69-75

36. Zahradnik RT, Moreno EC. Structural features of human dental enamel as revealed by isothermal water vapour sorption. Arch. Oral Biol. 1975; 20(5-6): 317-325.

---

* De acordo com as normas do PPGO/UFPB, baseadas na norma do International Committee of Medical Journal Editors - Grupo de Vancouver. Abreviatura dos periódicos em conformidade com o Medline.